Three-dimensional Computational Fluid Dynamics (CFD) Study of the Gas-particle Circulation Pattern within a Fluidized Bed Granulator: by Full-Factorial Design of Fluidization Velocity and Particle Size

Huolong Liu[1,2], Seongkyu Yoon[1], Mingzhong Li[2]

[1]Department of Chemical Engineering, University of Massachusetts Lowell, USA [2]School of pharmacy, De Montfort University, Leicester, UK

Corresponding author Huolong Liu E-mail: Huolong_Liu@uml.edu

Abstract

The fluidization velocity and mean particle size were selected to be numerically investigated pertaining to their effects on the gas-particle circulation pattern within a fluidized bed granulator by three-dimensional CFD simulation applying an Eulerian-Eulerian two-fluid model (EETFM). The CFD simulations were designed by full-factorial design method and the developed CFD model was experimentally validated. The fluidization process was proved to reach a quasi-steady state. The gas-particle circulation pattern and particle concentration distribution were analyzed based on fluidization velocity and mean particle size. A mathematical model was developed to provide guidance on how to change fluidization level during one experiment.

Graphical Abstract

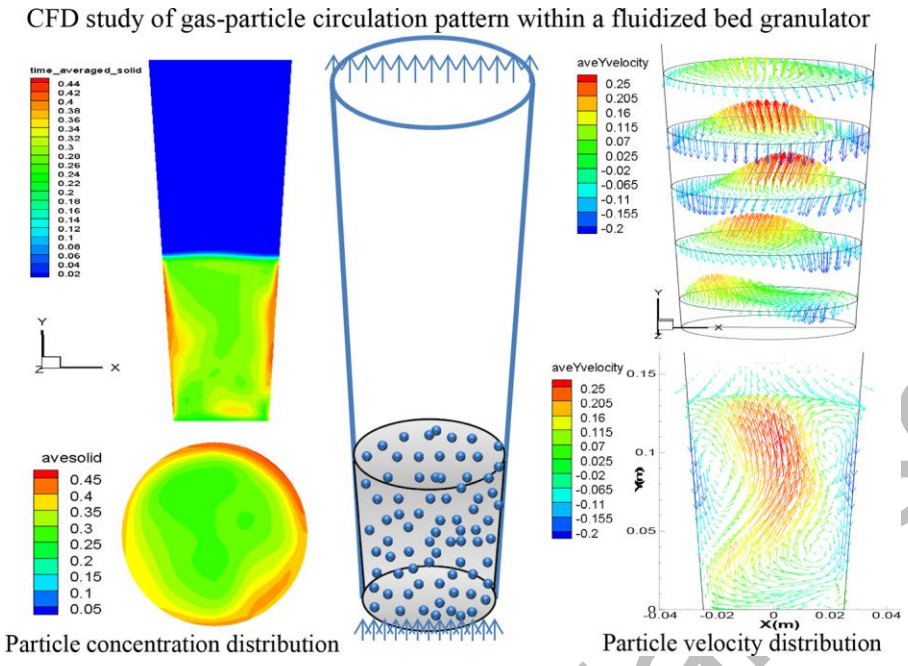

KEYWORDS: fluidized bed granulator; fluidization; computational fluid dynamics (CFD); gas-particle hydrodynamics; full-factorial design

1. INTRODUCTION

Spray fluidized bed granulation has been widely used in the pharmaceutical industry to produce granules to improve powder properties, such as flowability, dispersibiltiy and bulk density. The powders can be mixed, granulated and dried in the same equipment to minimize the equipment costs, loss of product during transfer and the possibility of cross-contamination. Over recent decades, fluidized bed granulation has been extensively studied due to its complexity and many interrelated process variables, which are mainly

divided into two categories according to the two main features of spray fluidized bed granulation: binder spraying and fluidization [1-8].

Recently, binder spraying parameters such as spray rate, atomization pressure and pulsed spray frequency, have been extensively studied [9-11]. In particular, adjusting the pulsed frequency of binder spray was shown to be an effective way of controlling the granule size during spray fluidized bed granulation, in which the liquid feed is interrupted in regular sequences that allows drying and rewetting of granules [11-13]. In the authors' previous work, a hybrid process model was developed by linking key operating variables, including spray rate, atomization pressure and pulsed frequency of binder spray, with the granule properties to predict granule growth in a batch granulation process [14]. A two-compartmental population balance model (TCPBM) was developed by considering the heterogeneity of the granulation process based on computational fluid dynamics (CFD) analysis of the fluidization within the spray fluidized bed granulation [15]. The TCPBM has demonstrated obvious advantages in predicting mean granule size compared to homogeneous based PBM, which indicates the importance of fluidization. Through stable fluidization, enhanced mass- and heat-transfer rates are provided during spray fluidized bed granulation, which is a special advantage compared to other conventional granulation methods. Solid circulation pattern within the fluidized bed granulator generates a specific mass, liquid and temperature distribution, which significantly controls the granulation mechanisms. Generally, the fluidization is significantly affected

by the operating conditions and evolution of granule properties [16, 17]. By literature reviewing and our previous experimental experience, the fluidization velocity and mean particle size were found to be the most critical parameters as representatives of operating conditions and granule properties, respectively [11].

Fluidization velocity is an important operating variable affecting both fluidization hydrodynamics and granule growth, and it plays key role in producing high powder mixing uniformity. The fluidization velocity can affect the granulation behavior and final particle size distribution by affecting the drying capacity [16]. At the initial stage of the granulation, it is reported that higher fluidization velocity produces a higher granule growth rate because of the higher frequency and energy of collisions between granules. However, larger granules were finally obtained from low fluidization velocity due to the small shear force at lower fluidization velocity [16, 17]. For a batch fluidized bed granulation process, it is inherently unstable, and sensitive to the bed humidity. If drying is insufficient, high humidity generated by less efficient fluidizing air flow during the granulation process could pose a danger of over-wetting of particles, resulting in a non-retrievable bed collapse [18, 19]. It has been found that the fluidization velocity should be adjusted to prevent the bed collapse during the spray fluidized bed granulation [20].

Particle size is another important granulation characteristic which plays a crucial role in fluidization. The average particle size increases under different granulation mechanisms during experiment, which results in different particle holdup and fluidization level within the granulator. Fan et al. claimed that gas-particle circulation pattern is strongly affected by particle size [21]. For glass beads with a size of 0.8-1 mm, the mean glass flow was predominantly upward on one side of the bed and downward as a return flow on the other side, while for the glass beads with a size of 250-450 μm, a typical UCDW (upwards along the center and downwards along the annulus) pattern can be observed. Laverman et al. [22] observed the same particle flow pattern for various types and a broad range of particle size and the difference was in the fluidization velocity at which the number of vortices changed. However, particle flow pattern was not found to be affected by the particle size [23-25].

A large number of experimental studies have been carried out regarding gas-particle flow pattern identification within spray fluidized bed granulation processes for different process parameters and physical properties. However, the complex hydrodynamics of fluidized bed granulation still need to be investigated for further understanding owing to complicated phenomena such as particle-particle, particle-droplet and particle-bubble interactions. Recently, computational fluid dynamics (CFD) has emerged as an effective tool for investigating gas-particle fluidized bed hydrodynamics. In literature, CFD has been widely applied for modeling multiphase flow of wet granulation process to reduce

the design time and cost [26-35]. In general, two different approaches of CFD modelling are used to model a gas-solid fluizied bed: the Eulerian-Eulerian approach, in which all phases are considered as interpenetrating continua and the Eulerian-Lagrangian approach in which at least one phase is considered as a discrete phase interacting with the other phases [30, 36-43]. To date, several models built upon the Eulerian-Lagrange framework have been developed such as the computational fluid dynamics-discrete element method (CFD-DEM), dense discrete phase model (DDPM) and multi-phase-particle-in-cell (MP-PIC) method. With the advance in computational resources and capacities, these methods become increasingly popular for the modelling of particulate flow and some study cases in fluidized bed could be found. However, because of the computational limitations of the Eulerian-Lagrange model which is normally limited to a relatively small number of particles, the Eulerian-Eulerian model is the preferred choice for simulating the gas-particle hydrodynamics of a fluidized bed. The effectiveness of the Eulerian-Eulerian model of CFD has been extensively validated by the experiments [30, 37, 38, 44].

Thus, the aim of this study is focused on providing an understanding of how the gas-particle circulation pattern and hydrodynamics within the spray fluidized bed granulation are influenced by the fluidization velocity and particle size by CFD simulation. The fluidization velocity was changed from 0.6 m^3/h to 1.8 m^3/h and the particle size was changed from 164 μm to 500 μm to simulate the granule growth

during granulation process. Both ranges for fluidization velocity and particle size are true values adopted from the authors' preliminary experimental work [11]. Based on these two variables, a total of 9 CFD simulations were designed by the full-factorial design method with three levels for each variable. The CFD model was solved in the software package of FLUENT 13.0 (Ansys Inc., USA) using the Eulerian-Eulerian approach by the kinetic theory of granular flow (KTGF) and was validated both experimentally and theoretically [45]. By changing the fluidization velocity and particle size in the simulation design, their effects on gas-particle circulation pattern, particle velocity distribution, particle concentration distribution, and particle circulation time were investigated, respectively. Finally, a mathematical model was developed to describe the relationship between particle circulation time, fluidization velocity and particle size, which provides guidance on how to change the fluidization level by adjusting the fluidization velocity during one experiment.

2. SIMULATION DESIGN AND EXPERIMENTAL SETUP

In this work, the particle circulation pattern is quantitatively represented by the particle circulation time. The granulation process is simulated by the increasing particle size and changing fluidization velocity in the simulation design. In order to investigate the relationship between the particle circulation pattern, fluidization velocity and particle size, CFD simulations were designed using the full-factorial design method and JMP 11.0 software (SAS, SAS Institute, Cary, NC, USA). A total of 9 CFD simulations were

designed with fluidization velocity and particle size as factors and each factor has three levels as shown in Table 1. The low, medium and high levels of each independent factor are determined based on the preliminary experimental study [11], which respectively represents the beginning, medium and final stages of the granulation process. A non-linear quadratic model was developed to describe the relationship between particle circulation time, fluidization velocity and particle size, which is given as:

$$Y = b_0 + b_1 x_1 + b_2 x_2 + b_{12} \quad x_1 - x_{1,mediate} \quad x_2 - x_{1,mediate} \tag{1}$$

$$x_{1,mediate} = \frac{x_{1,min} + x_{1,max}}{2} \tag{2}$$

$$x_{2,mediate} = \frac{x_{2,min} + x_{2,max}}{2} \tag{3}$$

Where, *Y* is a measured response associated with each factor's combination; b_0 is an intercept; b_1 to b_{12} are regression coefficients calculated from the observed experimental values of *Y*; x_1 and x_2 are the real values of independent variables and $x_{1,min}$, $x_{1,max}$ and $x_{2,min}$, $x_{2,max}$ are the minimum and maximum value of variable x_1 and x_2, respectively. The term $x_1 x_2$ represents the interaction effect.

Once the CFD simulations are designed, fluidization experiments are carried out. A lab-scale (46.5 g/batch) batch fluidized bed granulator (MP-MicroTM, GEA Process Engineering Ltd, UK) is used. The selected granulator and its geometry are illustrated in Figure 1. The conical fluidized bed granulator is made of transparent Plexiglas with inner-diameter of 4.97 cm at the bottom and 7.48 cm at the top. The height of the container

is 30 cm, which is high enough to prevent entrainment of the particles with outgoing gas. The air distributor is a 4500 mesh stainless steel plate at a constant temperature of 40 °C by an electrical heater before entering the bed for each experiment. Details about the fluidized bed granulator system could be found in our previous study [11]. The particles used for the fluidization are microcrystalline cellulose (MCC) with a density of 450 kg/m^3 supplied by Blackburn Distributions Ltd, UK. The size grades of 164 μm, 332 μm and 500 μm are used and the fluidization velocities are 0.6 m^3/h, 1.2 m^3/h and 1.8 m^3/h. For each experiment, the same amount of 46.5 g MCC is used. The fluidized bed granulator dimensions and material properties can be found in Table 2. For each of the simulations designed in this section, the specified fluidization velocity and particle size are used, and fluidized bed height are measured for model validation in section 5.

3. CFD MODELING OF A FLUIDIZED BED GRANULATOR

3.1 Computational Model

The present work aims at modelling multiphase flow, where an Eulerian-Eulerian two-fluid model (EETFM) is applied incorporating the kinetic theory of granular flow (KTGF). In this approach, the different phases are treated mathematically as interpenetrating continuums [46], where gas phase is defined as the primary phase and the particle phase is defined as the dispersed particulate phase. Conservation equations were derived for each phase and linked by interphase momentum transfer coefficients and pressure. The hydrodynamic model of gas-solid fluidized beds is based on the

conservation of mass and momentum. In the present study, the gas-solid two-phase flow is nonreactive, isothermal and transient. The two-fluid model (TFM) requires constitutive equations to describe the rheology of the solid phase. When the particle motion is dominated by collision interactions, the concepts from fluid kinetic theory can be introduced to describe the effective stresses in the solid phase resulting from particle streaming collision. Furthermore, these constitutive relations for the solid phase stress, based on the kinetic theory, were derived by Lun et al. [47], which have been accepted widely. A standard mixture $\mathrm{k}-\varepsilon$ model was used to solve the transport equations. The governing equations including mass and momentum conservation equation of gas and solid phase, constitutive equations, and closure relations used in this study are summarized in Table 3.

3.2 CFD Modeling Strategy

As described in the previous section, CFD simulations with an Eulerian-Eulerian two-fluid model (EETFM) were developed to study gas-particle circulation pattern within a fluidized bed granulator, which considers the conservation of mass and momentum for the gas and particle phases. The standard $k-\varepsilon$ model was used to describe the turbulence inside the fluidized bed granulator, where the kinetic theory of granular flow (KTGF) was employed in the momentum balance equation for the solid phase. The finite volume approach by a commercial CFD software package FLUENT 13.0 (Ansys Inc., US) was used for solving the computational model in a 3-D domain comprising all the interior

volume of the conical product chamber in the fluidized bed granulator in double precision mode. As described in section 2, the computational domain was discretized by unstructured hexahedrons using the commercial software ICEM CFD 13.0 (Ansys Inc., USA). First order upwind schemes in both space and time were used for the solution of the equations. A time step of 1×10^{-4} seconds with a maximum 200 iterations per time step was chosen. This iteration was adequate to achieve convergence at each time step. The convergence criterion was set to 1×10^{-3} for the relative error between two successive iterations for each scaled residual component. The phase coupled SIMPLE algorithm was used for the pressure-velocity coupling, in which the coupling terms were solved implicitly to form part of the solution matrix. The CFD simulations were performed on a 2 GHz Intel Four Core processor desktop computer with 4 GB RAM using a XP platform.

3.3 Initial And Boundary Conditions

In each CFD simulation of a fluidized bed, particles were assumed to be spherical and monodispersed. Based on the experiments, it was found that the bed height of the initial primary MCC particles was between 8 and 9 cm. The initial bed height of packed solid particles was therefore, set as 8.75 cm in the CFD simulations. The particle volume fraction was set as 0.53 based on the ratio of the volume of the actual primary particles used in the experiments and the initial bed volume packed in the simulations [11].

For the boundary conditions, the distributor was modeled as a porous plate placed at the bottom of the conical product chamber in which the uniform air was injected into the bed. The particles were not allowed to penetrate the distributor. The pressure-outlet was used as boundary condition at the top of the conical chamber, which was assumed to have a constant static atmospheric pressure as a reference operating pressure. A no-slip condition was set for walls, which means no momentum waste occurred when the air and solid collided with the wall. The restitution coefficient was set as 0.9 for the particles in the simulations. Configuration of the simulated fluidized bed and its boundary conditions are shown in Figure 1 and the details of parameters used in the simulations are given in Table 4.

3.4 Grid Sensitivity Analysis

An 'O' type unstructured hexahedron grid of fluidized bed was created using the commercial software ICEM CFD 13.0 (Ansys Inc., USA). Grid sensitivity analysis was carried out at three different grids with total cells of 60000, 101400, and 135000. The sensitivity of the predicted transient pressure drop, bed height as well as solid particle concentration to the cell number was investigated for a particle size of 164 μm and a fluidization velocity of 0.6 m^3 / h.

In Figure 2 (a, b), a grid with more than 101400 cells did not improve the accuracy of the predicted particle concentration, while a grid with 60000 cells generated a significantly

different particle concentration distribution. Pressure drop along the bed is defined as pressure at the bed inlet minus its value at the bed outlet. As reported in Figure 2 (c), predicted pressure drop along the bed is slightly affected by grids except for two large deviations predicted by the coarsest grid at 1.8 s and 3.7 s.

Furthermore, the height of the fluidizing bed surface at different grids was calculated and plotted in Figure 2 (d). The predicted bed height was clearly found to be dependent on the grids: Grids with 101400 and 135000 cells garnered close predictions of bed height evolution, while a grid with 60000 cells predicted an obviously small bed height after two seconds of simulation time. Therefore, the grid having 101400 cells was chosen as the optimum value to secure the highest accuracy and lowest computational cost.

3.5 Convergence To Quasi-Steady State

The CFD simulation in this study was carried out in transient mode. Although the solid flow in the fluidized bed is unsteady with changes of local velocity in both magnitude and direction during fluidization, it is important to ensure that the CFD simulation reaches a quasi-steady state, in which the gas-particle flow dynamics are generally time-independent. In order to determine the simulation time to the quasi-steady state, the fluidizing bed height and particle concentration distribution were monitored for simulation 1 shown in Figure 3.

It can be seen from Figure 3 (a) that the bed height increased quickly from 0.087 m to 0.14 m after 3 seconds, and remained approximately constant. Figure 3 (b) demonstrates the particle concentration distribution evolution at the starting period of fluidization. Initially, all the particles were packed at the bottom of fluidized bed. As the fluidizing air was injected, large air bubbles were formed at the air distributor, which forced the fluidized bed height to increase. At 0.6 s, the initially formed two large air bubbles reached the fluidizing bed surface and the fluidized bed height reached its maximum value. At that moment, the particle concentration had an inhomogeneous distribution, mainly distributing on the central column region and area close to the wall. Until 4 s, a relatively uniform particle concentration distribution has been reached and fluidized bed height came to a stable value at 0.14 m with bed expansion ratio of 61%.

It can be concluded that the quasi-steady state was reached after 4 s for simulation 1 because all parameters showed constant values. The time to reach the quasi-steady state differed between simulations. However, using the same method described above showed that all simulations designed in this study reached a quasi-steady state after 5 s. Therefore, the CFD simulation results are analyzed based on the time-averaged value from 5 s to 10 s throughout the paper.

4. RESULTS AND DISCUSSION

4.1 Validation Of CFD Model

The effectiveness of the CFD simulation is validated by both theoretical and experimental methods. Results of experiment 1 are given in Figure 4 as representative. The theoretical method is comparing the total pressure drops of the bed determined by theoretical predictions and numerical simulations [45]. It is well known that among all the parameters describing fluidized bed granulation performance, the pressure drop is the most important one, particularly in scale-up and design of fluidized bed granulators, making it an ideal variable to use for validation. At the minimum fluidization conditions, the powder in the bed is fully supported by the upward gas flow. The force generated by the upward gas is proportional with the pressure drop, which is mainly balanced by the weight of the solid bed. Therefore, the pressure drop across the bed is given as [45]:

$$\Delta P = \left(\rho_s - \rho_g\right)\left(1-\varepsilon_{mb}\right) g H_{mb} + \varepsilon_{mb}\rho_g g H_{mb} + \rho_g g \left(H_{chamber} - H_{mb}\right) \quad (30)$$

Where, ρ_s and ρ_g are the particle and air densities respectively, H_{mb} and ε_{mf} are the bed height and the bed voidage at the minimum fluidization velocity, and $H_{chamber}$ is the product chamber height.

Figure 4 (a) shows the comparison between the CFD predicted pressure drop and theoretically calculated value of 193.90 Pa. It is indicated that the overall pressure drop decreases at the beginning of fluidization and then fluctuates around a steady-state value of 187 Pa after 3 s. It can be seen that the steady-state value obtained by the CFD simulation is in reasonably good agreement with the theoretically calculated value with

prediction error of 3.6%, indicating that the CFD model can be used to predict the performance of a fluidized bed.

Figure 4 (b) illustrates the comparison between experimental and CFD predicted fluidized bed height, from which excellent match between them could be found. From the experiment, it is found that the bed height after reaching the quasi-steady state is 13 cm. The model predicted fluidized bed height changes between 13.25 and 13.75 cm, which provide an acceptable prediction error range of 1.9% - 5.8%.

4.2 Effect Of Fluidization Velocity And Particle Size On Particle Velocity Distribution

The time-averaged particle velocity vector fields for various fluidization velocities of small (164 μm), medium (332 μm) and large (500 μm) particles are depicted in Figures 5, 6 and 7, respectively. In order to investigate the particle circulation pattern within the 3D fluidized bed thoroughly, three types of particle velocity vector fields were included: a) on horizontal cross-section at 10%, 30%, 50%, 70% and 90% bed height, b) on vertical plane *XY*, c) on vertical plane *ZY*.

The effect of fluidization velocity on the particle circulation pattern at small particle size (164 μm) is given in Figure 5. It is clearly shown that solid particles move upward from the central region and flow downward along the wall for all fluidization velocities from

0.6 to 1.8 m^3/h, which has also been experimentally observed by Lin et al. [23]. Large vortices were observed randomly distributed in the area between central region and wall at lower fluidization velocity (0.6 m^3/h), and they are shrunk and break up into more small size vortices as the fluidization velocity increases to 1.8 m^3/h. For both upward moving particles and downward moving particles, maximum velocity was reached at middle bed height and minimum velocity was observed at top and bottom of fluidized bed. This could be explained by the interaction between particle weight and pressure drop along the bed height generated by the fluidizing air. The reason why the particles could remain fluidized in the bed is that the particle weight is balanced by drag force generated from the pressure drop. For upward flowing particles, on the lower half bed domain, where the drag force is larger than the particle weight, the particles are accelerated by the upward force difference, while the particle velocity starts to decrease where the drag force is smaller than particle weight on the upper half bed domain. The same theory can be utilized to explain the particle velocity evolution for the downward flowing particles.

Figure 6 shows the influence of fluidization velocity on particle circulation pattern at medium particle size of 332 μm. Firstly, smaller average particle velocity was shown compared to that in Figure 5 at each fluidization velocity, which could be explained by the increased particle weight. At lower fluidization velocity (from 0.6 m^3/h to 1.2

m^3/h), an identical stable particle circulation pattern was indicated by all types of particle velocity vector fields, where particles moved upward from central region and fell downward along the wall, forming large vortices between them. In the meantime, small particle vortices were observed at the corner between wall and air distributor, which indicated the moving trail of particles accumulating in this region. At high fluidization velocity (1.8 m^3/h), a new particle circulation pattern occurred where solid particles moved upward along plane *XY* and fell downward along plane *ZY*, shown in Figure 6 (c). From Figure 6 (c), it was indicated that both small and long vortices appeared simultaneously and located randomly at any position within the fluidized bed but not only at area between the central region and wall.

The influence of fluidization velocity on particle circulation pattern at large particle size of 500 μm is shown in Figure 7. Further reduced average particle velocity was observed due to further increased particle weight. It was found that the same particle circulation patterns as in Figure 6 (c) happened for all fluidization velocities at particle size of 500 μm, where almost all particles are moving upward along *XY* plane and fell downward to the air distributor along the *ZY* plane. At a lower fluidization velocity of 0.6 m^3/h, laminar particle flow was found and only two large symmetric vortices appeared on the *ZY* plane. As fluidization velocity increased, the particle flow became more turbulent and the large vortices were forced to break into small vortices. The upward moving particles

brought by the arising bubbles conflicted with the dropping particles by the splashed air bubbles, creating a sharp interior boundary.

4.3 Effect Of Fluidization Velocity And Particle Size On Particle Concentration Distribution

Figure 8 shows the time-averaged solid concentration contour on the cross-sectional plane at different bed heights for simulations of all fluidization velocities and particle sizes. The cross-section plane was created at 10%, 30%, 50%, 70% and 90% of bed height. It is indicated that an obviously high particle concentration was distributed on the annulus area against the wall where particles fell downward and low particle concentration was found on the central region where particles moved upward. This phenomenon can explain the difference between the upward and downward particle velocity, because high particle concentration generates high frictional force between particles and obstructs the increase of downward particle velocity. For smaller particle size of 164 μm, the simulation results showed that particles are most likely concentrated at the middle section domain of the bed, while for particle size of 332 μm and 500 μm, particles are likely concentrated at the upper section domain of the bed. At the small particle size of 164 μm in Figure 8 (a), the particle concentration distribution changes slightly with increasing fluidization velocity. Time-averaged particle concentration distributions at all fluidization velocities are small, which could be explained by the sufficient fluidization due to small particle size. However, at the medium particle size of

332 μm in Figure 8 (b) and the large particle size of 500 μm in Figure 8 (c), the particle concentration decreased significantly as the fluidization velocity increased. For medium (332 μm) and large (500 μm) particles, obvious higher particle concentrations were observed on each cross-section planes comparing to that of small particles (164 μm).

The effect of particle size and fluidization velocity on the particle concentration distribution at the vertical plane *XY* is also investigated as shown in Figure 9. The fluidized bed expansion increases with fluidization velocity for all the particle sizes. As the fluidization velocity increases, bubbles appear initially at the bottom of granulator and increase in both number and size, which is clearly observed for particles of 332 μm and 500 μm in size. However, the bubbles distorted significantly and merge frequently at high fluidization velocity, which generates twisty bubbles as shown in Figure 9 (b) and (c). It can also be seen that the fluidized bed expansion decreases as particle size increases. Under the same fluidization velocity, more bubbles and a heterogeneous fluidization state are generated by the larger particle size.

4.4 Determination Of Particle Circulation Time Model For A Fluidized Bed Granulator

In the fluidized bed granulator, the particle circulation pattern is an important design attribute for either process scale-up or experiment design. The particle circulation pattern can be utilized to explain the aggregation and breakage phenomena. In this section, the

particle circulation time is considered as an indicator of the particle circulation pattern and is modelled as function of the fluidization velocity and particle size.

The particle circulation time in the present study is defined as the sum of time required for the particles to reach the bed surface and to return back to the air distributor, as described by Rowe [48, 49]:

$$t_c = \frac{V_{upward}}{\overline{v}_{upward}} + \frac{V_{downward}}{\overline{v}_{downward}} \quad (31)$$

Where, V_{upward} and $V_{downward}$ are the total upward flowing particle volume and total downward flowing particle volume, respectively. $\overline{v}_{upward}$ and $\overline{v}_{downward}$ are the average upward particle volume flow rate and average downward particle volume flow rate, respectively.

$$V_{upward} = \sum_{v_i>0} \varepsilon_{s,i} * v_i \quad (32)$$

$$V_{downward} = \sum_{v_i<0} \varepsilon_{s,i} * v_i \quad (33)$$

And

$$\overline{v}_{upward} = \sum_{k=1}^{n\_k} \sum_{s_{vi} \in surface\ y=h_k} \varepsilon_{s,i} * s_{vi} * \vartheta_{i\_y\_up} / n\_k \quad (34)$$

$$\overline{v}_{downward} = \sum_{k=1}^{n\_k} \sum_{s_{vi} \in surface\ y=h_k} \varepsilon_{s,i} * s_{vi} * \vartheta_{i\_y\_down} / n\_k \quad (35)$$

$$h_k = \left(k - 0.5\right) * H_{chamber} / 120 \quad (36)$$

Where, v_i is the cell volume; $\varepsilon_{s,i}$ is the time-averaged solid volume fraction of the cell v_i; s_{vi} is the cross-section area of the cell v_i with the horizontal surface $y = h_k$; $\vartheta_{i\_y\_up}$ is the particle velocity in cell v_i on the surface through which particle moves upward; $\vartheta_{i\_y\_down}$ is the particle velocity in cell v_i on the surface through which particle moves downward; and n_k is the grid number along y-axis.

Using this method, the particle circulation time was calculated for all the nine CFD simulations and given in Table 1 as dependent variables Y_1. Figure 10 shows the effect of fluidization velocity and particle size on the particle circulation time in the fluidized bed. It can be seen that the circulation time decreases with fluidization velocity while increases with particle size. Three CFD simulations run 1, run 5 and run 9 with particle size of 164 μm, 332 μm, and 500 μm, respectively, are marked on Figure 10, which indicate that the particle circulation time can be kept constant by adjusting the fluidization velocity as particle size increases from 164 μm to 500 μm. In addition, the fitted linear function from run 1, run 5 and run 9 provides a slope value of -0.21 close to zero with R^2 value of 0.9. For the simulation 7 with a particle size 500 μm and fluidization velocity 0.6 m^3/h, an apparently high circulation time 4.61 s is observed, which indicates the occurring of particle bed de-fluidization. From the authors' previous experimental study [11], it is known that the final particle mean size has a range from 290 μm to 734 μm. therefore, the initial fluidization velocity of 0.6 m^3/h has to be increased to avoid the de-fluidization phenomena.

The process model parameters of b_0, b_1, b_2, and b_{12} in equation (1) were obtained using JMP 11 software (SAS, SAS Institute, Cary, NC, USA). A mathematical model of the particle circulation time in terms of fluidization velocity and particle size is developed, given as follows:

$$t_c = 3.08 + 2.66\times10^{-3} * d_{s,m} - 1.07 * v_{a,inlet} - 4.32\times10^{-3} * d_{s,m} - 332 * v_{a,inlet} - 1.2 \quad (37)$$

Where, $d_{s,m}$ is the mean particle diameter in μm and $v_{a,inlet}$ is the fluidization velocity in m^3/h. If the particle size distribution can be obtained online during an experiment, the particle circulation time can be fixed at T_c by adjusting the fluidization velocity in following algorithm:

$$v_{a,inlet} = \frac{1.359 + 7.84\times10^{-3} d_{s,m} - T_c}{4.32\times10^{-3} d_{s,m} - 0.3642} \quad (38)$$

5. CONCLUSIONS

In the present work, an Eulerian-Eulerian two-fluid model (EETFM) integrating the kinetic theory of granular flow (KTGF) was developed to simulate the gas-particle circulation pattern within the fluidized bed granulator. The CFD simulations were designed by full-factorial design method and were performed using software ANSYS Fluent 13.0. The influence of fluidization velocity and particle size on the particle circulation pattern was investigated thoroughly with ranges from 0.6 m^3/h to 1.8

m^3/h and from 164 μm to 500 μm, respectively. It was found that large vortices were driven to shrink or split into small vortices by increasing the fluidization velocity, making the particle flow more turbulent at high levels of fluidization velocity. By increasing the particle size, average particle velocity was reduced and a different particle circulation pattern was found at the highest level of particle size (500 μm), where particles moved upward along the trajectory of *XY* plane and fell downward to the air distributor along the trajectory of *ZY* plane. For particle velocity, both the upward and downward moving particles were found to reach the highest velocity at middle bed height and have smaller velocity on the two sides of fluidized bed, which can be explained by the interaction of particle weight and bed pressure drop. It was indicated that an obviously high particle concentration was distributed on the annulus area against the wall where particles fell downward and low particle concentration was found on the central region through where particles moved upward. The particle circulation time, as symbol of particle circulation pattern, within the fluidized bed was proved to be constant by adjusting the fluidization velocity as the particle size increased. A mathematical model of the particle circulation time in terms of fluidization velocity and particle size was developed, which provides guidance on how to change the fluidization level by adjusting the fluidization velocity during one experiment.

NOMENCLATURE

C_D	Drag coefficient
d_s	Particle diameter (m)
e_s	Particle-particle restitution coefficient, dimensionless
$\vec{g}$	Gravitational acceleration (m/s^2)
g_0	Radial distribution coefficient, dimensionless
$H_{chamber}$	product chamber height (m)
H_{mb}	bed height at the minimum fluidization velocity (m)
$\bar{\bar{I}}$	Identity matrix
K_{gs}	Inter-phase momentum transfer coefficient ($kg/m^3 s$)
k_{Θ_s}	Diffusion coefficient for granular energy (kg/ms)
ΔP	pressure drop across the bed (Pa)
p_s	Dispersed phase (particulate) pressure (Pa)
$R_{downward}$	Downward particle volume flow rate (m^3/s)
Re_s	Particle Reynolds number
R_{upward}	Upward particle volume flow rate (m^3/s)
t_c	Particle circulation time (s)
$\vec{v_g}$	Gas velocity (m/s)
$\vec{v_s}$	particle velocity (m/s)
$v_s^{'}$	Fluctuation velocity of particles (m/s)

Greek symbols

α_g	Volume fraction of gas phase
α_s	Volume fraction of solid phase
α_{smax}	Maximum volume fraction of solid phase
μ_g	Viscosity of gas phase ($Pa \bullet s$)
μ_s	Solid shear viscosity ($Pa \bullet s$)
ρ_g	Density of gas phase (kg / m^3)
ρ_s	Density of solid phase (kg / m^3)
$\bar{\bar{\tau}}_g$	Shear stress for gas phase (N / m^2)
$\bar{\bar{\tau}}_s$	Shear stress for solid phase (N / m^2)
λ_s	Solid bulk viscosity ($Pa \bullet s$)
ε_{mf}	bed porosity at the minimum fluidization velocity
γ_{Θ_s}	collision dissipation of energy ($kg / (s^3 m)$)
Θ_s	Granular temperature (m^2 / s^2)
θ	Angle of internal friction
φ_{gs}	Transfer rate of kinetic energy ($kg / (s^3 m)$)

Subscripts

g	gas phase
s	solid phase
m	mixture

REFERENCES

1. Iveson, S.M., et al., *Nucleation, growth and breakage phenomena in agitated wet granulation processes: a review.* Powder Technology, 2001. **117**(1–2): p. 3-39.

2. Reynolds, G.K., et al., *Breakage in granulation: A review.* Chemical Engineering Science, 2005. **60**(14): p. 3969-3992.

3. Rajniak, P., et al., *A combined experimental and computational study of wet granulation in a Wurster fluid bed granulator.* Powder Technology, 2009. **189**(2): p. 190-201.

4. Ramkrishna, D., *Population Balances. Theory and applications to particulate systems in engineering.* . 2000, New York: Academic Press.

5. Li, Z., et al., *Coupled CFD-PBE Simulation of Nucleation in Fluidized Bed Spray Granulation.* Drying Technology, 2013. **31**(15): p. 1888-1896.

6. da Silva, C.A.M. and O.P. Taranto, *Real-Time Monitoring of Gas–Solid Fluidized-Bed Granulation and Coating Process: Evolution of Particle Size, Fluidization Regime Transitions, and Psychometric Parameters.* Drying Technology, 2015. **33**(15-16): p. 1929-1948.

7. Grünewald, G., B. Westhoff, and M. Kind, *Fluidized Bed Spray Granulation: Nucleation Studies with Steady-State Experiments.* Drying Technology, 2010. **28**(3): p. 349-360.

8. Link, K.C. and E.-U. Schlünder, *Fluid1zed Bed Spray Granulation And Film Coating A New Method For The Investigation Of The Coating Process On A Single Sphere.* Drying Technology, 1997. **15**(6-8): p. 1827-1843.

9. Loh, Z.H., et al., *Spray granulation for drug formulation.* Expert Opinion on Drug Delivery, 2011. **8**(12): p. 1645-1661.

10. Faure, A., P. York, and R.C. Rowe, *Process control and scale-up of pharmaceutical wet granulation processes: a review.* European Journal of Pharmaceutics and Biopharmaceutics, 2001. **52**(3): p. 269-277.

11. Liu, H., et al., *Using the Box–Behnken experimental design to optimise operating parameters in pulsed spray fluidised bed granulation.* International Journal of Pharmaceutics, 2013. **448**(2): p. 329-338.

12. Ehlers, H., et al., *Granule size control and targeting in pulsed spray fluid bed granulation.* International Journal of Pharmaceutics, 2009. **377**(1&2): p. 9-15.

13. Närvänen, T., et al., *Controlling granule size by granulation liquid feed pulsing.* International Journal of Pharmaceutics, 2008. **357**(1&2): p. 132-138.

14. Liu, H. and M. Li, *Population balance modelling and multi-stage optimal control of a pulsed spray fluidized bed granulation.* International Journal of Pharmaceutics, 2014(a). **468**(1-2): p. 223-233.

15. Liu, H. and M. Li, *Two-compartmental population balance modeling of a pulsed spray fluidized bed granulation based on computational fluid dynamics (CFD) analysis.* International Journal of Pharmaceutics, 2014(b). **475**(1–2): p. 256-269.

16. Hemati, M., et al., *Fluidized bed coating and granulation: influence of process-related variables and physicochemical properties on the growth kinetics.* Powder Technology, 2003. **130**(1–3): p. 18-34.

17. Bouffard, J., M. Kaster, and H. Dumont, *Influence of Process Variable and Physicochemical Properties on the Granulation Mechanism of Mannitol in a Fluid Bed Top Spray Granulator.* Drug Development and Industrial Pharmacy, 2005. **31**(9): p. 923-933.

18. Quevedo, J.A., et al., *Evaluation of assisting methods on fluidization of hydrophilic nanoagglomerates by monitoring moisture in the gas phase.* Chemical Engineering Science, 2007. **62**(9): p. 2608-2622.

19. Teunou, E. and D. Poncelet, *Batch and continuous fluid bed coating - review and state of the art.* Journal of Food Engineering, 2002. **53**(4): p. 325-340.

20. Ronsse, F., J. Depelchin, and J.G. Pieters, *Particle surface moisture content estimation using population balance modelling in fluidised bed agglomeration.* Journal of Food Engineering, 2012. **109**(3): p. 347-357.

21. Fan, X., Z. Yang, and D.J. Parker, *Impact of solid sizes on flow structure and particle motions in bubbling fluidization.* Powder Technology, 2011. **206**(1–2): p. 132-138.

22. Laverman, J.A., et al., *Experimental study on the influence of bed material on the scaling of solids circulation patterns in 3D bubbling gas–solid fluidized beds of glass and polyethylene using positron emission particle tracking.* Powder Technology, 2012. **224**: p. 297-305.

23. Lin, J.S., M.M. Chen, and B.T. Chao, *A novel radioactive particle tracking facility for measurement of solids motion in gas fluidized beds.* AIChE Journal, 1985. **31**(3): p. 465-473.

24. Mostoufi, N. and J. Chaouki, *On the Axial Movement of Solids in Gas-Solid Fluidized Beds.* Chemical Engineering Research and Design, 2000. **78**(6): p. 911-920.

25. Pallarès, D. and F. Johnsson, *A novel technique for particle tracking in cold 2-dimensional fluidized beds—simulating fuel dispersion.* Chemical Engineering Science, 2006. **61**(8): p. 2710-2720.

26. Zhong, W.Q., et al., *Discrete Element Method Simulation of Cylinder-Shaped Particle Flow in a Gas-Solid Fluidized Bed.* Chemical Engineering & Technology, 2009. **32**(3): p. 386-391.

27. Chalermsinsuwan, B., P. Kuchonthara, and P. Piumsomboon, *Effect of circulating fluidized bed reactor riser geometries on chemical reaction rates by using CFD simulations.* Chemical Engineering and Processing: Process Intensification, 2009. **48**(1): p. 165-177.

28. Utikar, R.P. and V.V. Ranade, *Single jet fluidized beds: Experiments and CFD simulations with glass and polypropylene particles.* Chemical Engineering Science, 2007. **62**(1-2): p. 167-183.

29. Vaishali, S., S. Roy, and P.L. Mills, *Hydrodynamic simulation of gas-solids downflow reactors.* Chemical Engineering Science, 2008. **63**(21): p. 5107-5119.

30. Taghipour, F., N. Ellis, and C. Wong, *Experimental and computational study of gas - solid fluidized bed hydrodynamics.* Chemical Engineering Science, 2005. **60**(24): p. 6857-6867.

31. Al-Rashed, M., et al., *Multiphase CFD modeling: Fluid dynamics aspects in scale-up of a fluidized-bed crystallizer.* Chemical Engineering and Processing: Process Intensification, 2013. **63**: p. 7-15.

32. Li, Z., et al., *CFD Simulation on Drying and Dust Integration in Fluidized Bed Spray Granulation.* Drying Technology, 2012. **30**(10): p. 1088-1098.

33. Sae-Heng, S., T. Swasdisevi, and M. Amornkitbamrung, *Investigation of Temperature Distribution and Heat Transfer in Fluidized Bed Using a Combined CFD-DEM Model.* Drying Technology, 2011. **29**(6): p. 697-708.

34. Jaskulski, M., P. Wawrzyniak, and I. Zbiciński, *CFD Model of Particle Agglomeration in Spray Drying.* Drying Technology, 2015. **33**(15-16): p. 1971-1980.

35. Wawrzyniak, P., et al., *Modeling of Dust Explosion in the Industrial Spray Dryer.* Drying Technology, 2012. **30**(15): p. 1720-1729.

36. Fries, L., et al., *DEM–CFD modeling of a fluidized bed spray granulator.* Chemical Engineering Science, 2011. **66**(11): p. 2340-2355.

37. Grace, J.R. and F. Taghipour, *Verification and validation of CFD models and dynamic similarity for fluidized beds.* Powder Technology, 2004. **139**(2): p. 99-110.

38. Acosta-Iborra, A., et al., *Experimental and computational study on the bubble behavior in a 3-D fluidized bed.* Chemical Engineering Science, 2011. **66**(15): p. 3499-3512.

39. Freireich, B., et al., *Incorporating particle flow information from discrete element simulations in population balance models of mixer-coaters.* Chemical Engineering Science, 2011. **66**(16): p. 3592-3604.

40. Dosta, M., S. Antonyuk, and S. Heinrich, *Multiscale Simulation of Agglomerate Breakage in Fluidized Beds.* Industrial & Engineering Chemistry Research, 2013. **52**(33): p. 11275-11281.

41. Kumar, A., et al., *Model-based analysis of high shear wet granulation from batch to continuous processes in pharmaceutical production – A critical review.* European Journal of Pharmaceutics and Biopharmaceutics, 2013. **85**(3, Part B): p. 814-832.

42. Hosseini, S.H., M. Zivdar, and R. Rahimi, *CFD simulation of gas–solid flow in a spouted bed with a non-porous draft tube.* Chemical Engineering and Processing: Process Intensification, 2009. **48**(11–12): p. 1539-1548.

43. Chalermsinsuwan, B., P. Kuchonthara, and P. Piumsomboon, *CFD modeling of tapered circulating fluidized bed reactor risers: Hydrodynamic descriptions and chemical reaction responses.* Chemical Engineering and Processing: Process Intensification, 2010. **49**(11): p. 1144-1160.

44. Sánchez-Delgado, S., et al., *Estimation and experimental validation of the circulation time in a 2D gas–solid fluidized beds.* Powder Technology, 2013. **235**(0): p. 669-676.

45. Lettieri, P., et al., *CFD modelling of liquid fluidized beds in slugging mode.* Powder Technology, 2006. **167**(2): p. 94-103.

46. Anderson, T.B. and R. Jackson, *Fluid mechanical description of fluidized beds. Equations of motion.* Industrial & Engineering Chemistry Fundamentals, 1967. **6**(4): p. 527-539.

47. Lun, C.K.K., et al., *Kinetic theories for granular flow: inelastic particles in Couette flow and slightly inelastic particles in a general flow field.* Journal of Fluid Mechanics, 1984. **vol. 140**: p. p.223-256.

48. Ronsse, F., J. Depelchin, and J.G. Pieters, *Particle surface moisture content estimation using population balance modelling in fluidised bed agglomeration.* Journal of Food Engineering. **109**(3): p. 347-357.

49. Rowe, P.N., *Estimation of solids circulation rate in a bubbling fluidised bed.* Chemical Engineering Science 1973. **28**(3): p. 979-980.

Table 1 Variables, levels and response in the full-factorial CFD simulation design

Run	Independent variables			Dependent variables
	Mode	X_1 (μm)	X_2 (m^3/h)	Y_1 (s)
1	−−	164	0.6	2.57
2	−0	164	1.2	2.22
3	−+	164	1.8	2.02
4	0−	332	0.6	3.23
5	00	332	1.2	2.37
6	0+	332	1.8	2.22
7	+−	500	0.6	4.61
8	+0	500	1.2	2.56
9	++	500	1.8	2.32

Table 2 Apparatus dimensions and material parameters

Parameters	Value
Bed geometry	
$H_{chamber}\,(cm)$	30
$D_{inlet}\,(cm)$	4.97
$D_{outlet}\,(cm)$	7.48
Solid phase properties (MCC)	
$\rho_s\,(kg/m^3)$	450
$d_s\,(\mu m)$	164, 332, 500
Gas phase properties	
$\rho_g\,(kg/m^3)$	1.225
$\mu_g\,(kg/m\bullet s)$	1.79×10^{-5}
$u_f\,(m^3/h)$	0.6, 1.2, 1.8

Table 3 Detailed governing, constitutive and closure equation in simulation

Continuity equations for gas and solid
$\frac{\partial\ \alpha_g\rho_g}{\partial t}+\nabla\bullet\ \alpha_g\rho_g\vec{v}_g\ =0$ (4)
$\frac{\partial\ \alpha_s\rho_s}{\partial t}+\nabla\bullet\ \alpha_s\rho_s\vec{v}_s\ =0$ (5)
Conservation of momentum of gas and solid
$\frac{\partial\ \alpha_g\rho_g\vec{v}_g}{\partial t}+\nabla\bullet\ \alpha_g\rho_g\vec{v}_g\vec{v}_g\ =-\alpha_g\nabla p+\nabla\bullet\ \alpha_g\bar{\bar{\tau}}_g\ +K_{gs}\ \vec{v}_s-\vec{v}_g\ +\alpha_g\rho_g\vec{g}$ (6)
$\frac{\partial\ \alpha_s\rho_s\vec{v}_s}{\partial t}+\nabla\bullet\ \alpha_s\rho_s\vec{v}_s\vec{v}_s\ =-\alpha_s\nabla p-\nabla p_s+\nabla\bullet\ \alpha_s\bar{\bar{\tau}}_s\ +K_{gs}\ \vec{v}_g-\vec{v}_s\ +\alpha_s\rho_s\vec{g}$ (7)
Gas phase/solid phase stress tensors
$\bar{\bar{\tau}}_g=\mu_g\ \nabla\vec{v}_g+\nabla\vec{v}_g^{\ T}$ (8)
$\bar{\bar{\tau}}_s=\mu_s\ \nabla\vec{v}_s+\nabla\vec{v}_s^{\ T}\ +\alpha_s\left(\lambda_s-\frac{2}{3}\mu_s\right)\nabla\bullet\vec{v}_s\bar{\bar{I}}$ (9)
Bulk solid viscosity
$\lambda_s=\frac{4}{3}\alpha_s\rho_s d_s g_0\ 1+e_s\ \sqrt{\frac{\Theta_s}{\pi}}$ (10)
Algebraic granular temperature equation

$$0 = -p_s \bar{\bar{I}} + \bar{\bar{\tau}}_s : \nabla \vec{v}_s - \gamma_{\Theta_s} \quad (11)$$

Collision dissipation of energy

$$\gamma_{\Theta_s} = \frac{12\ 1-e_s^2\ g_0}{d_s\sqrt{\pi}} \rho_s \alpha_s^2 \Theta_s^{1.5} \quad (12)$$

$$\Theta_s = \frac{1}{3}\overline{v_s' v_s'} \quad (13)$$

Solid pressure

$$p_s = \alpha_s \rho_s \Theta_s \left[1 + 2g_0 \alpha_s\ 1+e_s\ \right] \quad (14)$$

Radial distribution function

$$g_0 = \left[1 - \left(\frac{\alpha_s}{\alpha_{smax}}\right)^{1/3}\right]^{-1} \quad (15)$$

Shear viscosity of solid

$$\mu_s = \mu_{s,col} + \mu_{s,kin} + \mu_{s,fin} \quad (16)$$

Collisional viscosity

$$\mu_{s,col} = \frac{4}{5}\alpha_s \rho_s d_s g_0\ 1+e_s \sqrt{\frac{\Theta_s}{\pi}} \quad (17)$$

Kinetic viscosity

$$\mu_{s,kin} = \frac{10\rho_s d_s \sqrt{\Theta_s \pi}}{96\alpha_s g_0\ 1+e_s}\left[1 + \frac{4}{5}\alpha_s g_0\ 1+e_s\ \right]^2 \quad (18)$$

Frictional viscosity

$$\mu_{s,fin} = \frac{p_s \sin\theta}{2\sqrt{I_{2D}}} \quad (19)$$

Interphase drag force

$$k_{gs} = \frac{3}{4} C_D \frac{\alpha_s \alpha_g \rho_g \left| \vec{v}_s - \vec{v}_g \right|}{d_s} \alpha_g^{-2.65} \quad for\ \alpha_g > 0.8 \tag{20}$$

$$k_{gs} = 150 \frac{\alpha_s^2 \mu_g}{\alpha_g d_s^2} + 1.75 \frac{\alpha_s \rho_{g|\vec{v}_s - \vec{v}_g|}}{d_s} \quad for\ \alpha_g \le 0.8 \tag{21}$$

$$C_D = \frac{24}{\alpha_g Re_s} \left[1 + 0.15\ \alpha_g Re_s^{\ 0.687} \right] \tag{22}$$

$$Re_s = \frac{\rho_g d_s \left| \vec{v}_s - \vec{v}_g \right|}{\mu_g} \tag{23}$$

Turbulence model

$$\frac{\partial}{\partial x}\ \rho_m k\ + \nabla \bullet\ \rho_m k \vec{v}_m\ = \nabla \bullet \left(\frac{\mu_{t,m}}{\sigma_\varepsilon} \nabla k \right) + G_{k,m} - \rho_m \varepsilon \tag{24}$$

$$\frac{\partial}{\partial x}\ \rho_m \varepsilon\ + \nabla \bullet\ \rho_m \varepsilon \vec{v}_m\ = \nabla \bullet \left(\frac{\mu_{t,m}}{\sigma_\varepsilon} \nabla \varepsilon \right) + \frac{\varepsilon}{k}\ C_{1\varepsilon} G_{k,m} - C_{2\varepsilon} \rho_m \varepsilon \tag{25}$$

Mixture density and velocity

$$\rho_m = \sum_{i=1}^{N} \alpha_i \rho_i \tag{26}$$

$\vec{v}_m = \frac{\sum_{i=1}^{N} \alpha_i \rho_i \vec{v}_l}{\sum_{i=1}^{N} \alpha_i \rho_i}$ (27)
Turbulent viscosity
$\mu_{t,m} = \rho_m C_\mu \frac{k^2}{\varepsilon}$ (28)
Turbulent kinetic energy
$G_{k,m} = \mu_{t,m} \left[\nabla \vec{v}_m + \left(\nabla \vec{v}_m \right)^T \right] : \nabla \vec{v}_m$ (29)

Table 4 Parameters used in the CFD simulation

Property	Value
Initial bed height (cm)	8.75
Initial solid packing	0.53
Maximum solid volume fraction	0.63
Particle restitution coefficient	0.9
Time step (s)	0.0001
Convergence criteria	1.0×10^{-3}
Operating pressure (Pa)	101325
Maximum iterations every step	200

Figure 1 Configuration and computational grid of the fluidized bed granulator used in CFD simulations.

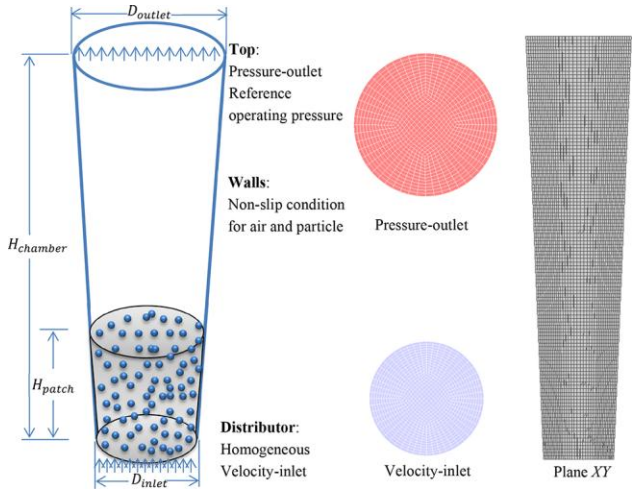

Figure 2 Mesh sensitivity study results; a) Solid volume fraction on cross-section plane *XY*; b) Solid volume fraction on cross-sectional plane *YZ*; c) Pressure drop; and d) Bed height.

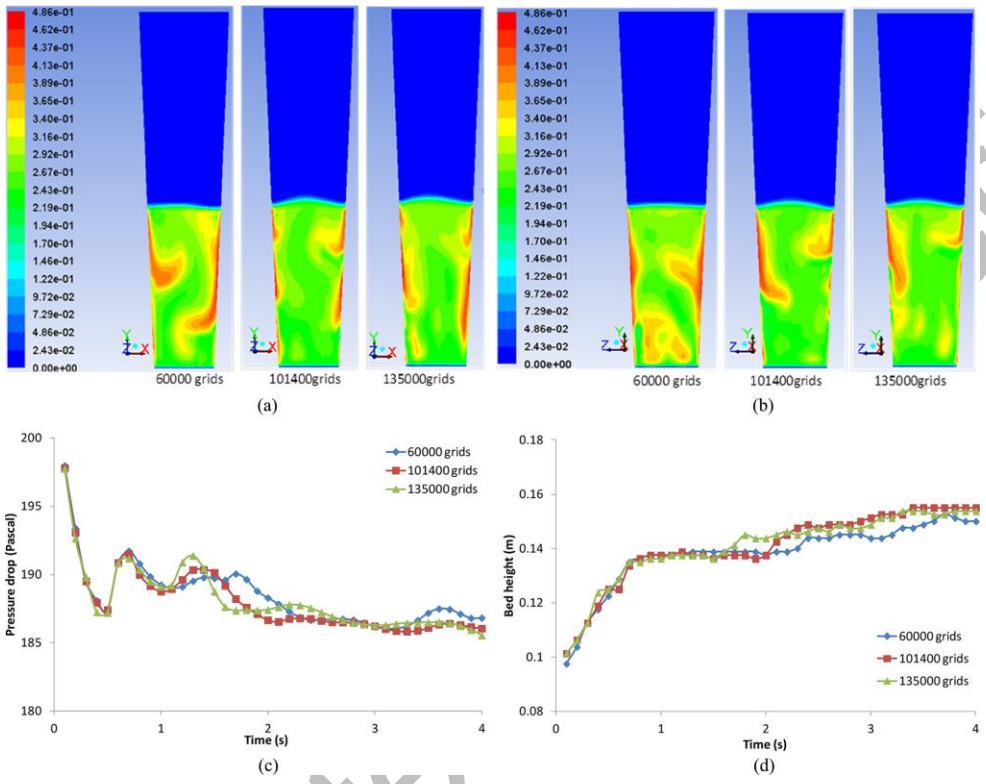

Figure 3 Convergence to quasi-steady state for CFD simulation: a) Bed height; b) Solid concentration distribution on the cross-section plane *XY*.

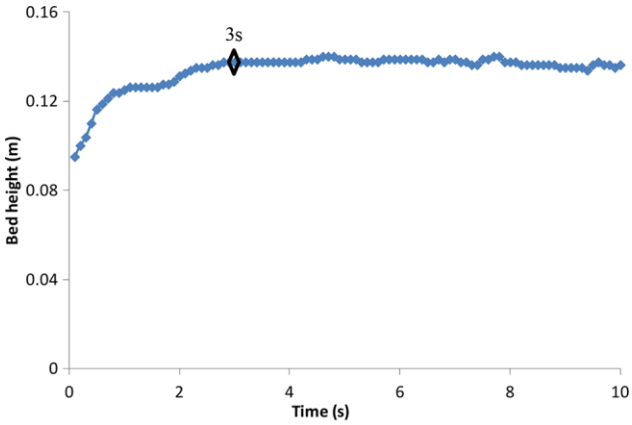

(a)

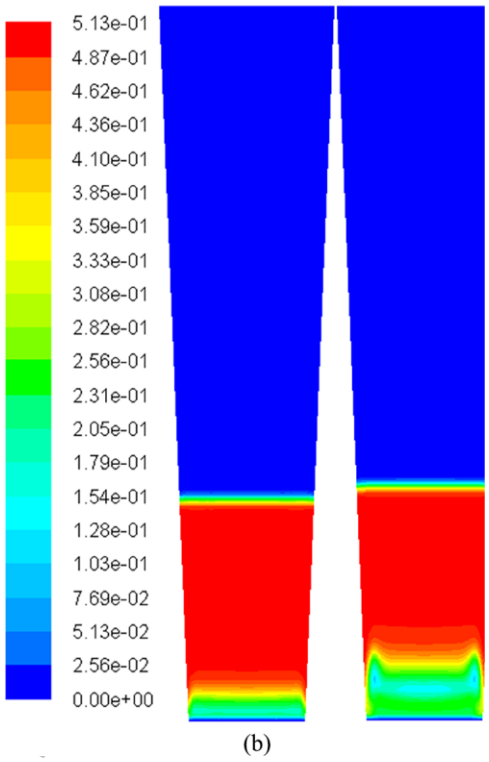

(b)

Figure 4 CFD model validation: a) Comparison of predicted bed pressure drop (blue diamond) with theoretically calculated value (red solid line); b) Comparison between experimental (red solid line) and CFD predicted fluidized bed height (blue diamond).

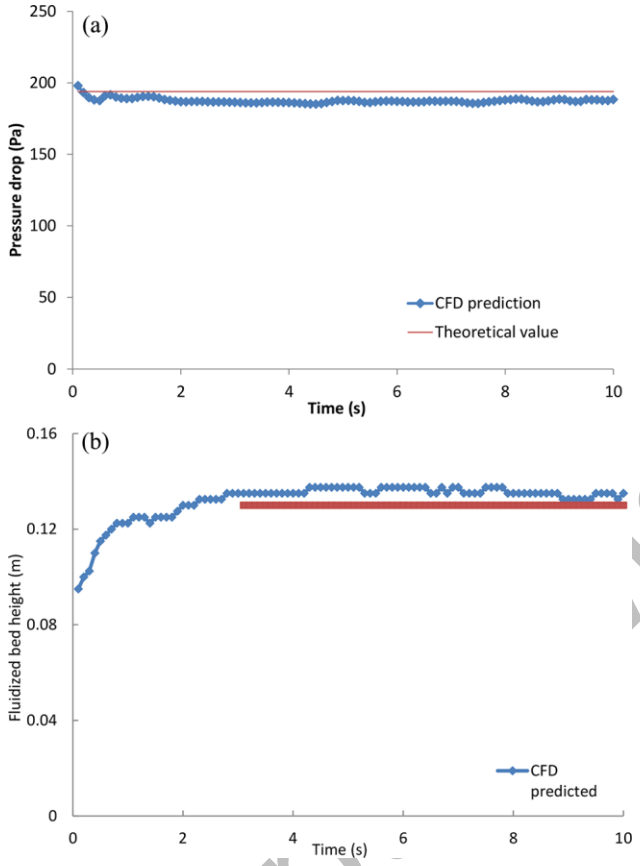

Figure 5 Particle velocity vector plot when particle size D=164 μm at fluidization velocity: a) 0.6 m^3/h, b) 1.2 m^3/h, and c) 1.8 m^3/h.

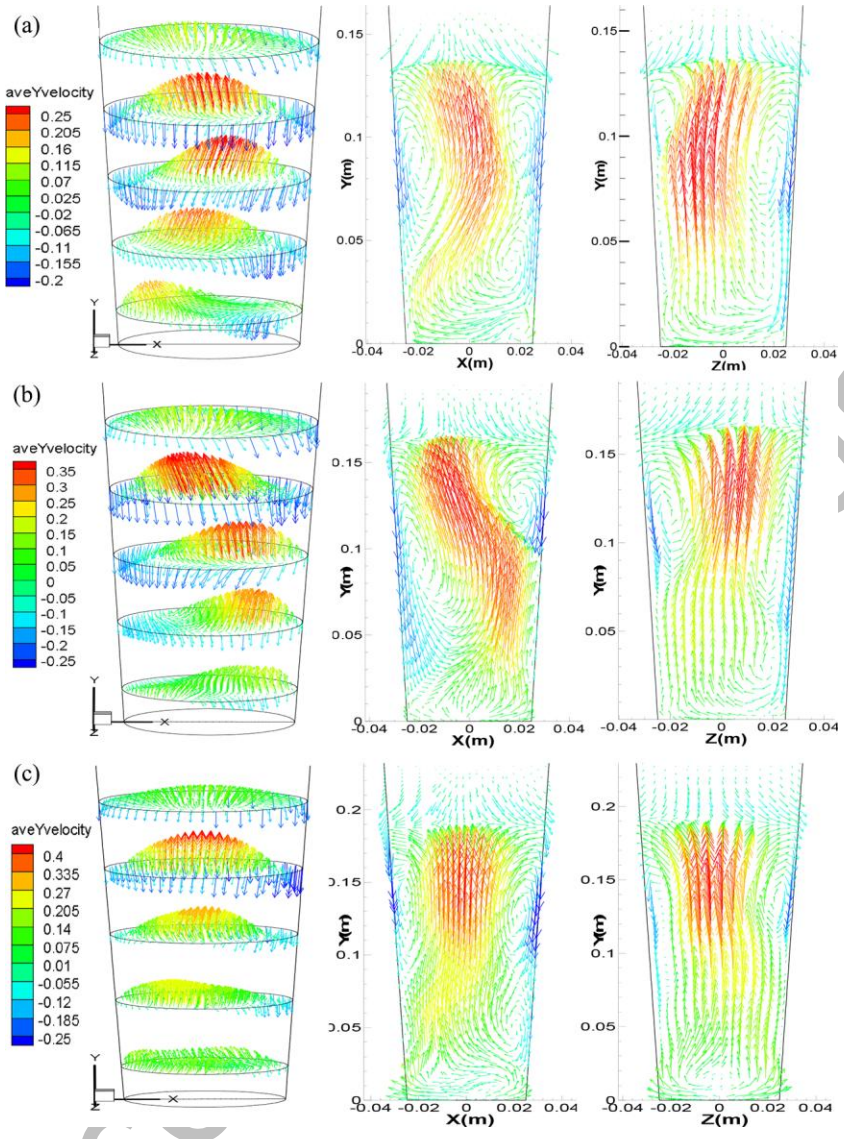

Figure 6 Particle velocity vector plot when particle size D=332 μm at fluidization velocity: a) 0.6 m^3/h, b) 1.2 m^3/h, and c) 1.8 m^3/h.

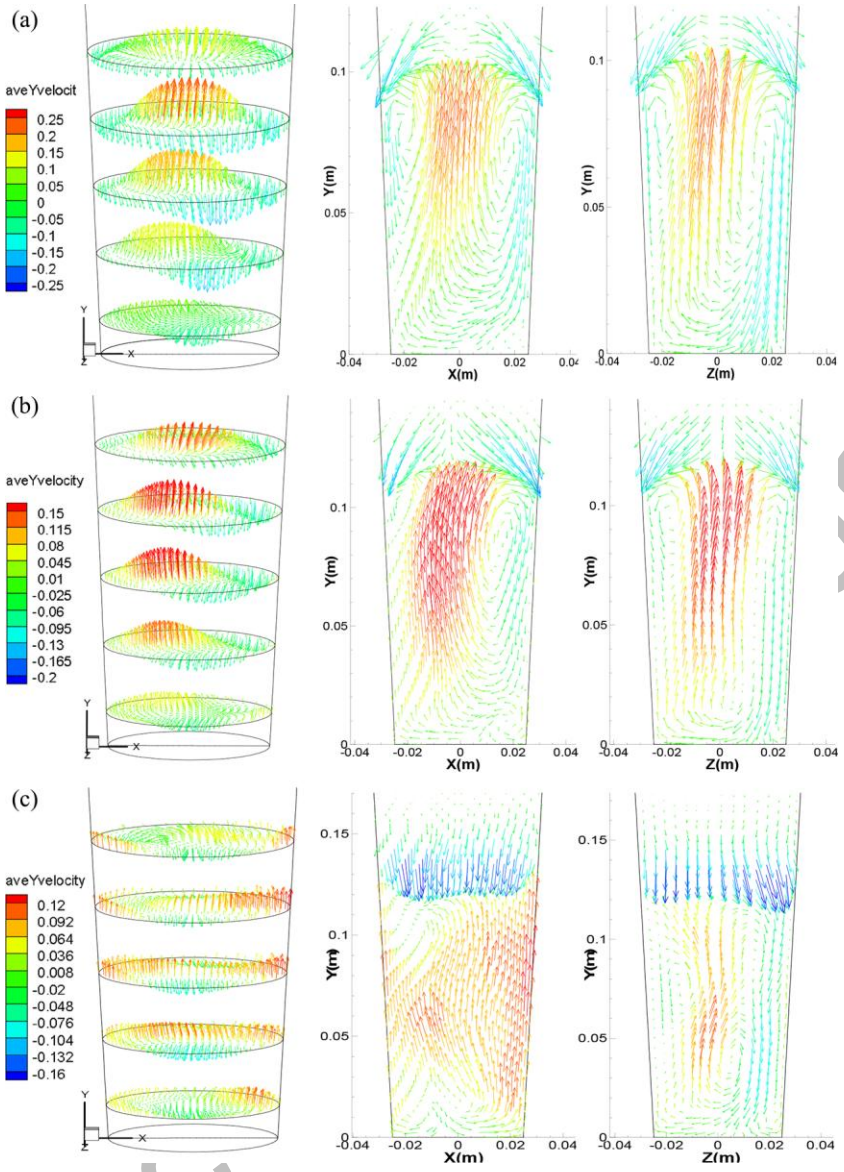

Figure 7 Particle velocity vector plot when particle size D=500 μm at fluidization velocity: a) 0.6 m^3/h, b) 1.2 m^3/h, and c) 1.8 m^3/h.

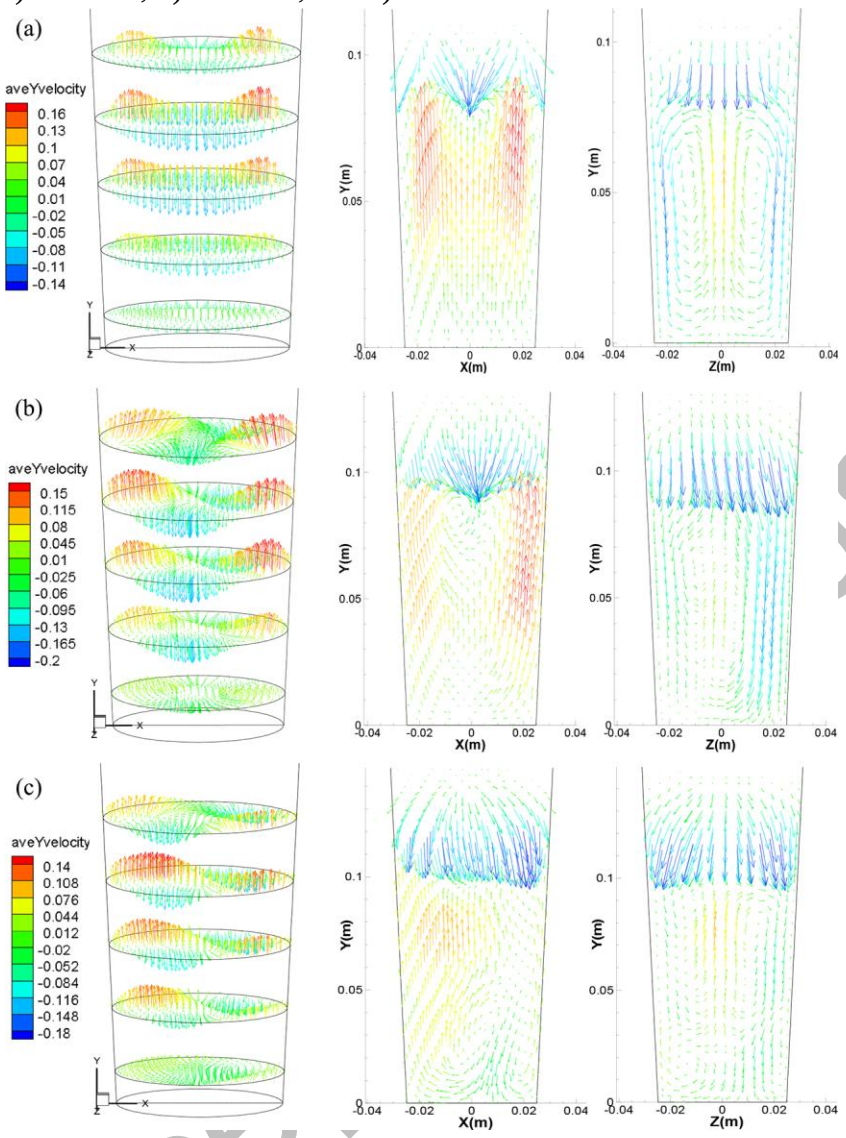

Figure 8 Time-averaged solid concentration distribution at horizontal cross-section planes of 10%, 30%, 50%, 70% and 90% of bed heights: a) particle size of 164 μm, b) particle size of 332 μm, and c) particle size of 500 μm.

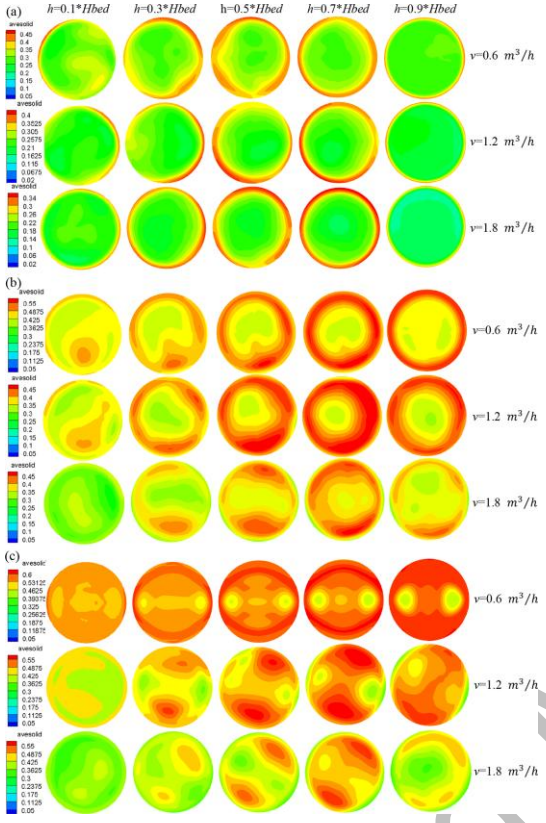

Figure 9 Time-averaged particle concentration distribution at vertical cross-section plane XY: a) particle size of 164 μm, b) particle size of 332 μm, and c) particle size of 500 μm.

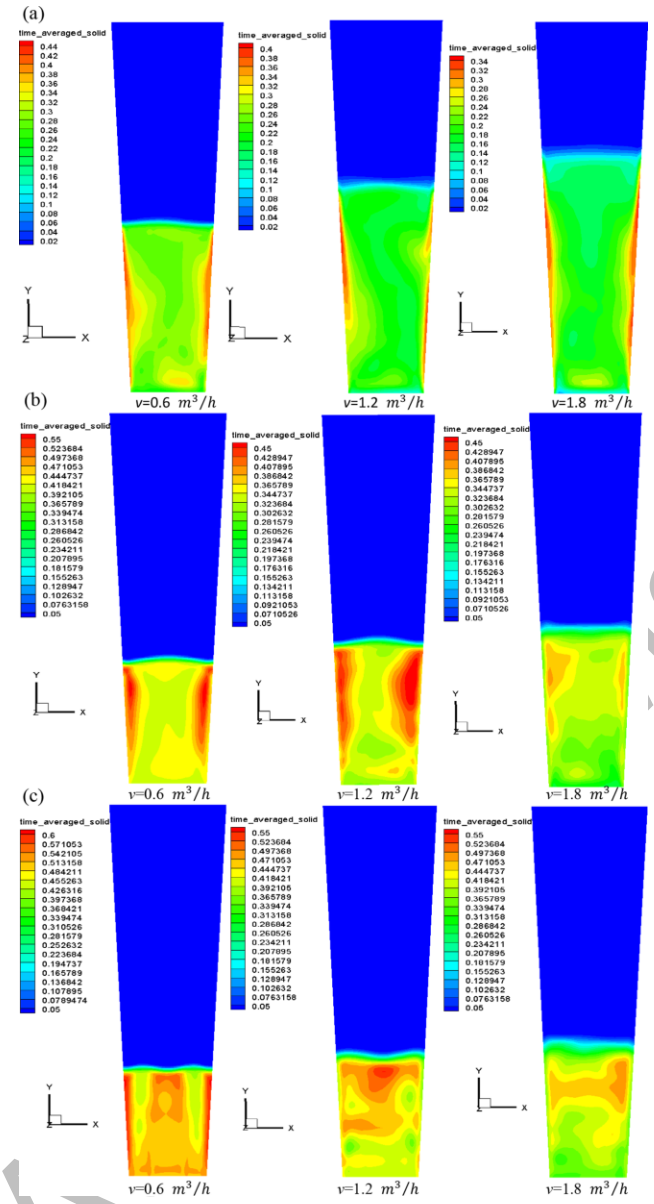

Figure 10 Particle circulation time with fluidization velocity under different particle size